



The role of mesoscale convective systems in the diurnal cycle of rainfall and its seasonality over sub-Saharan Northern Africa

Weiran Liu¹ · Kerry H. Cook¹ · Edward K. Vizy¹

Received: 25 May 2017 / Accepted: 28 February 2018 / Published online: 10 March 2018
© Springer-Verlag GmbH Germany, part of Springer Nature 2018

Abstract

This study evaluates the role of MCSs in the total rainfall distribution as a function of season from a climatological perspective (1998–2014) over sub-Saharan northern Africa and examines how the diurnal cycle of rainfall changes with season. Tropical Rainfall Measuring Mission (TRMM) 3B42V7 rainfall estimates and European Centre for Medium-Range Weather Forecasts ERA-Interim reanalysis are used to evaluate the climatology. The percentages of the full TRMM precipitation delivered by MCSs have meridional structures in spring, fall and winter, ranging from 0 to 80% across sub-Saharan northern Africa, while the percentages are homogenous in summer (> 80%). The diurnal cycles of MCS-associated precipitation coincide with the full TRMM rainfall. Attributes of MCSs, including size, count, and intensity, vary synchronously with the diurnal cycle of rainfall. The diurnal peaks are classified into three categories: single afternoon peak, continuous afternoon peak, and nocturnal peak. Single afternoon peaks dominate in spring and fall while continuous afternoon and nocturnal peaks are more common in summer, indicating the seasonality of the diurnal cycle. The continuous afternoon peak combines rainfall from two system types—one locally-generated and one propagating. The seasonality of the diurnal cycle is related to the seasonality of MCS lifetimes, and propagation speeds and directions. The moisture component of the MSE profile contributes to the instability most in summer when convection is more frequent. Low-level temperature, which is related to surface warming and sensible heat fluxes, influences the instability more during winter and spring.

Keywords MCS · Diurnal cycle of precipitation · SAHEL rainfall · African wave disturbances · African easterly waves · West Africa · Moist static energy

1 Introduction

Improved precipitation prediction over sub-Saharan northern Africa is important because this region experiences intense rainfall events that impact agriculture and the economic infrastructure, and regularly threaten lives. It is critical to understand the diurnal cycle of precipitation for simulating and predicting both total rainfall and extreme rainfall events in this region.

Heavy rainfall over sub-Saharan northern Africa is usually related to the generation of mesoscale convective systems (MCSs). Past studies (Laurent et al. 1998; Laing et al. 1999; Mathon et al. 2002; Mohr 2004) indicate that MCSs

contribute up to 95% of the boreal summer rainfall over this region, and the diurnal cycle of rainfall is associated with MCS activity.

While previous studies diagnose the role of MCSs in total rainfall, they consider only individual, or a small number, of summer seasons. One purpose of this study is to evaluate the role of MCSs in the total rainfall distribution as a function of season from a climatological perspective (1998–2014). Our analysis domain is a large interior region of sub-Saharan northern Africa, including the Sahel. In addition, we examine how the diurnal cycle of rainfall changes with season over the annual cycle, and evaluate the role of MCSs in this change. These results expand on previous studies that are limited to the summer season, as only a few case studies have focused on dry season (Knippertz and Fink 2008, 2009). Thus, to our knowledge, this is the first attempt to comprehensively analyze MCSs and the diurnal cycle of rainfall over the annual cycle for the interior region of sub-Saharan northern Africa.

✉ Weiran Liu
wrlu@utexas.edu

¹ Department of Geological Sciences, Jackson School of Geosciences, The University of Texas at Austin, 1 University Station C1100, Austin, TX, USA

Previous studies of MCS activity and its relationship to the diurnal cycle of rainfall over Africa are reviewed in Sect. 2. Section 3 presents the data and methodology used in this paper. Results are discussed in Sect. 4, followed by conclusions in Sect. 5.

2 Background

MCSs are commonly identified by the areal extent and intensity of precipitation. For example, Houze (1993) defined a MCS as a cloud system that connects with an ensemble of thunderstorms and produces a contiguous area of precipitation with a horizontal scale of 100 km or more in at least one direction. Mohr and Zipser (1996) defined an MCS as an area of 2000 km² or more with a brightness temperature at or below 225 K. Later studies (Nesbitt et al. 2000; Nesbitt and Zipser 2003; Jackson et al. 2009) adopt this definition.

The characteristics of mesoscale convection over Africa are generally not as well understood compared to convection over other continents. Due to limitations of the meteorological network in Africa, satellite data remains the primary source of observations. Precipitation observations from NASA's Tropical Rainfall Measurement Mission (TRMM, Huffman et al. 2007) satellite have been used in a number of studies of MCSs. For example, Nesbitt and Zipser (2003) identified individual storms within the combined TRMM dataset and found that the most intense precipitation features of MCSs peak around 1500 LT.

The MCSs over Africa are associated with the studies of rainfall. Past studies (Laurent et al. 1998; Laing et al. 1999; Mathon et al. 2002; Mohr 2004) indicate that MCSs contribute up to 95% of the boreal summer rainfall over this region, and the diurnal cycle of rainfall is associated with MCS activity. The diurnal cycle of rainfall across West Africa has peaks in late afternoon to early evening (Yang and Slingo 2001). Mohr (2004) examined the diurnal cycle of precipitation in sub-Saharan Africa for May–September, 1998–2001, concluding that the mean wet season diurnal cycle of precipitation evolves from a bimodal, highly-variable diurnal cycle north of 15°N to a unimodal, diurnal cycle with much less variability south of 10°N. In contrast, Zhang et al. (2016a) showed most regions of West Africa (98% in the climatology and 78% in 2006) have a single diurnal peak of rainfall either in the afternoon or at night.

Past studies examine MCS characteristics and diagnose their role in producing summer rainfall (Laurent et al. 1998; Laing et al. 1999; Mathon et al. 2002; Mohr 2004), while only a few case studies expand into the dry seasons. Knipertz and Fink (2008) provided synoptic and dynamical analysis during the dry seasons of 2003/04, while Knipertz and Fink (2009) presented a statistical evaluation

of dry-season wet events covering 23 dry seasons during 1979/80–2001/02.

Mohr (2004) investigated the diurnal variability of rainfall and found that it is primarily influenced by the frequency and life cycles of organized convective systems. As for the initiation of MCSs, numerous studies highlight the role of topography for African MCSs as mountain ranges help to initiate long-lived MCSs (Burpee 1972; Hodges and Thorncroft 1997; Laing et al. 2008). Large-scale topography plays a critical role in the spatial and diurnal patterns of convection, lightning, and rainfall (Jackson et al. 2009). Even modest rises in regional elevation can also provide the focal point for the initiation of convection (Vizy and Cook 2017). Convection can be triggered by heating over the elevated terrain, and/or at low-level convergent frontal boundaries such as those associated with sea/land breezes, lake breezes (Laing et al. 2011), gust fronts/cold pool outflow boundaries (Taylor et al. 2013; Birch et al. 2014a, b; Maurer et al. 2016), or the inter-tropical front (ITF; Eldridge 1957; Vizy and Cook 2017), which separates moisture-laden air flowing off the tropical Atlantic into West Africa from the dry, northerly Sahel/Saharan flow.

MCS initiation and development are also associated with atmospheric instability. The geographic and diurnal variability of moist convection over Africa reflects the importance of CAPE and vertical wind shear in the development of the systems (Hodges and Thorncroft 1997; Mohr and Thorncroft 2006; Laing et al. 2008; Janiga and Thorncroft 2014). Zhang et al. (2016a, b) concluded that afternoon rainfall peaks are associated with an unstable atmosphere, and that nocturnal rainfall peaks are associated with the westward propagation of rainfall systems.

Besides, convection over Africa is related with large-scale jets and waves. For example, past studies (Fortune 1980; Landsea and Gray 1992; Cook 1999; Crétat et al. 2015; Gaye et al. 2005; Hsieh and Cook 2005, 2007, 2008; Hopsch et al. 2010) indicate that the mid-tropospheric African easterly jet and African easterly waves (AEWs) play a role on the rainfall over Africa. AEWs influence the evolution of convection (Payne and McGarry 1977; Machado et al. 1993). Meanwhile, MCSs tend to occur ahead of or concurrent with the AEW trough (Reed et al. 1977; Duvel 1989; Diedhiou et al. 1999; Fink and Reiner 2003). Vertical shear related to the African easterly jet influences the location of intense convective systems (Mohr and Thorncroft 2006; Laing et al. 2008). Pu and Cook (2010, 2012) found the low-level West African westerly jet is associated with the moisture transport from the Atlantic onto the West African and influences the Sahel rainfall variations.

MCSs propagate after they are generated when the system remains in air that is potentially unstable enough that the outflows can trigger new convection. Laing et al. (2008) found that precipitating convective systems initiated over

elevated terrain propagate westward over sub-Saharan Africa and undergo cycles of regeneration. Organized convection in Africa consists of coherent sequences or episodes that span an average distance of about 1000 km and last about 25 h with the phase speed of 10–20 m/s. Laing et al. (2011) investigate coherent episodes of convection resulting from the regeneration of convection while propagating westward. These episodes have an average duration of 17.6-h and a span of 673-km; most have zonal phase speeds of 8–16 m/s. Vizy and Cook (2017) indicate that MCSs originated during the afternoon have phase speeds range between 8 and 14 m/s while the MCS phase speed is 7 m/s for nighttime genesis events.

In summary, a large portion of warm season rainfall over Africa has been associated with MCSs in previous studies. Either afternoon or nocturnal peaks are found in the diurnal cycle depending on location. Here we examine the role of MCSs in the diurnal cycle of rainfall from a more climatological view (1998–2014). We consider the seasonality of the diurnal cycle of precipitation, and how are MCSs related to these seasonal changes.

3 Datasets and methodology

The analysis domain for this study extends from 0°–30°E and 8°N–16°N (Fig. 1). This domain is selected because it is a large land region of sub-Saharan northern Africa that is removed from prominent mountain ranges that have elevations over 2000 m, such as the Ethiopian Highlands (35–40°E, 8–14°N), and the coast. However, our domain still includes elevated terrain, such as the Marraha Mountains (26.5°E, 15.5°N) and the Jos Plateau (7–10°E, 10–12°N).

The primary MCS-identification method for this study uses NASA TRMM 3B42V7 merged high quality (HQ)/Infrared (IR) rainfall estimates (Huffman et al. 2007). TRMM 3B42V7 is a high resolution (0.25°) product that

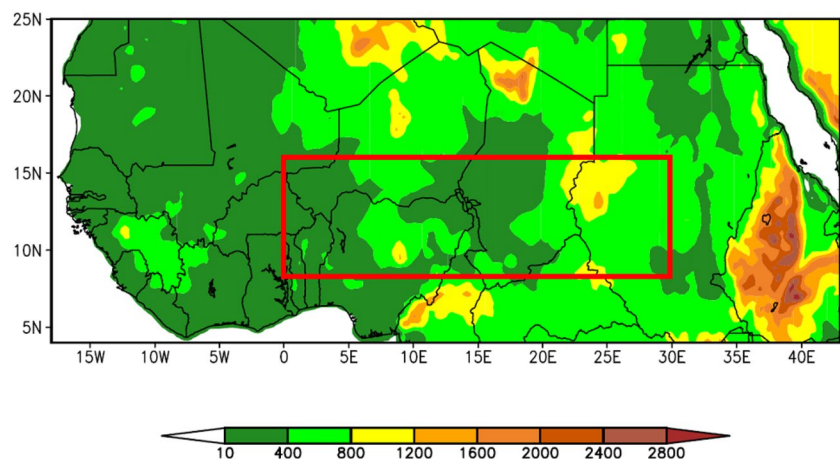
provides 3-hourly, multi-satellite rainfall estimates from January 1998 to present using the TRMM 3B42 algorithm.

MCSs are identified in the 3-hourly TRMM 3B42V7 using a two-step procedure that is based loosely on past MCS estimates (e.g., Maddox 1980; Houze 1993; Laing and Fritsch 1993; Mohr and Zipser 1996; Hodges and Thorncroft 1997; Laing et al. 1999; Mohr et al. 1999; Jirak et al. 2003). The first step is to select precipitation features for each 3-h timestep using a threshold rain rate, which is 25 mm/day. We test the sensitivity to this choice by assuming different thresholds, such as 10 and 50 mm/day. The threshold value chosen does not make a large difference in the number of MCSs identified, nor change the patterns of MCSs. In the TRMM 3B42V7 rainfall, 70–90% of sub-Saharan Northern African rainfall occurs at or above the 25 mm/day rate, so the selection of this threshold produces MCS counts that are roughly consistent with estimates from other studies (Mohr et al. 1999; Mathon et al. 2002). We also use a higher threshold, 100 mm/day, to evaluate the dependence of the results on the choice of the threshold and to understand if the most extreme rainfall events exhibit similar seasonal and diurnal cycles.

The second step in the MCS identification process is to apply a contiguous-area size criterion. Since past studies (e.g., Houze 1993; Mohr and Zipser 1996; Nesbitt and Zipser 2003) suggest that MCSs have minimum contiguous areas of about 2000 km², we require that there be at least three adjacent grid cells that meet the rainfall threshold in order to be identified as an MCS. At the resolution of TRMM 3B42V7 this corresponds to an area of 2000–2300 km², depending on latitude.

The University of Utah precipitation and cloud feature database (UtahPF; Nesbitt et al. 2000, 2006; Liu et al. 2008) was also considered for comparison. While UtahPF is valuable for examining precipitation features and providing information for evaluating MCS characteristics (Nesbitt et al. 2000, 2006; Liu et al. 2008; Liu and Zipser 2009; Jiang and

Fig. 1 Terrain elevation (meters) from the US Geological Survey (USGS) digital elevation model (DEM) interpolated to 30-km resolution. The yellow box denotes the analysis region. Black contours show country outlines



Zipser 2010; Jiang et al. 2011), this database is not designed for analyzing the spatial distribution of rainfall, which is the purpose of this study.

To better understand various characteristics of MCSs, we examine MCSs from two aspects. One is based on MCS counts, and the other is based on precipitation rates. Table 1 lists the acronyms and descriptions utilized for the analysis of TRMM 3B42V7 rainfall datasets. The term MCS-precipitation refers to TRMM 3B42V7 rainfall in the adjacent grid cells of identified MCSs.

The 6-hourly European Centre for Medium-Range Weather Forecasts ERA-Interim reanalysis (ERA-Interim; Dee et al. 2011) is used to evaluate the atmospheric dynamics fields.

In our analysis of seasonality, four seasons defined are boreal winter from November–March (NDJFM), spring from April–May (AM), summer from June–September (JJAS), and autumn, represented by October (Oct). These seasons were chosen by examining the percentage of the full TRMM precipitation delivered by MCSs in individual months (not shown) and combining months with similar spatial distributions. The NDJFM mean is selected as winter months since the percentage of the full TRMM precipitation delivered by MCSs in these months is below than 10% over more than half of analysis domain, with higher percentages (> 50%) located over the southern part of the analysis domain. April and May are similar. Specifically, the percentage is above 50% over more than half of the domain and low percentages (< 30%) occur in the vicinity of (15°E, 15°N). In June–September, a high percentage (80% or above) of the full TRMM precipitation is delivered by MCSs over more than 90% of the domain. October is chosen to represent fall, and is similar to April–May.

4 Results

4.1 Sensitivity to MCS selection criteria

Figure 2 shows the total number of MCSs over the sub-Saharan northern Africa domain (18°W–43°E, 4–25°N) for the T25 and T100 counts for 1998–2014. The MCSs' spatial distributions are similar in the two different estimates. The total number of MCSs decreases with increasing latitude,

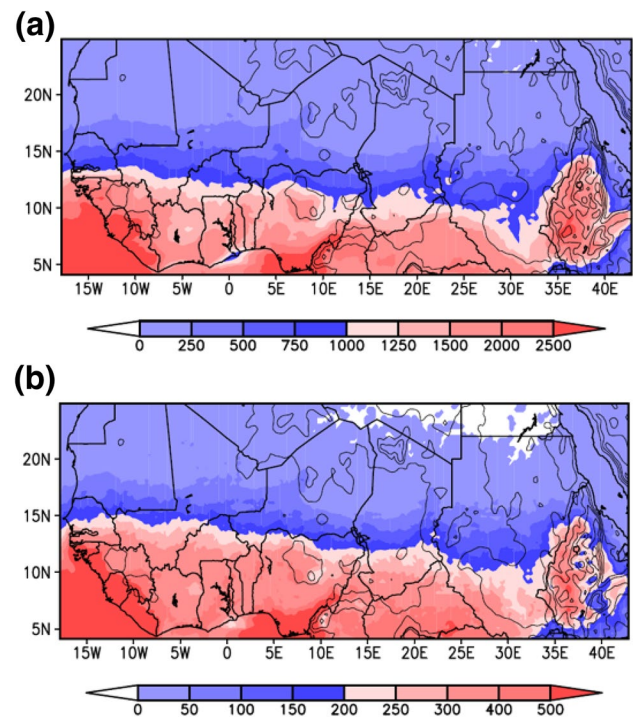


Fig. 2 Total number of MCSs from TRMM 3B42V7 using **a** the 25 mm/day threshold and **b** the 100 mm/day threshold. Black contours show country outlines

with a strong meridional gradient concentrated over the Sahel between 10°N and 16°N, depending on longitude. In both datasets, maxima are located along the Atlantic coast of Guinea, Sierra Leone, and Liberia, near the Jos Plateau (7–10°E, 10–12°N), west of the Cameroon Highlands (~10°E, 7°N), and over the Ethiopian Highlands (35–40°E, 8–14°N).

While there is similarity in the spatial distributions, the total numbers of MCSs in the T25 count and the T100 count vary considerably. The maximum of the T25 count exceeds 2500 MCSs while the T100 count has a maximum of around 500.

Differences between the MCS criteria can be better understood by examining one period of a typical summer day, namely, August 16, 2006. We tested other days in multiple years and found similar results. Figure 3a shows the

Table 1 Acronyms and descriptions utilized for the analysis of TRMM 3B42V7 rainfall datasets

Acronym	Description
T25 count	Count of TRMM 3B42V7 MCSs when applying a 25 mm/day threshold
T25 precipitation	Estimated TRMM 3B42V7 precipitation associated with T25 count MCSs
T100 count	Count of TRMM 3B42V7 MCSs when applying a 100 mm/day threshold
T100 precipitation	Estimated TRMM 3B42V7 precipitation associated with T100 count MCSs
full TRMM precipitation	Total TRMM 3B42V7 precipitation, including rainfall associated with MCSs and other rainfall event types

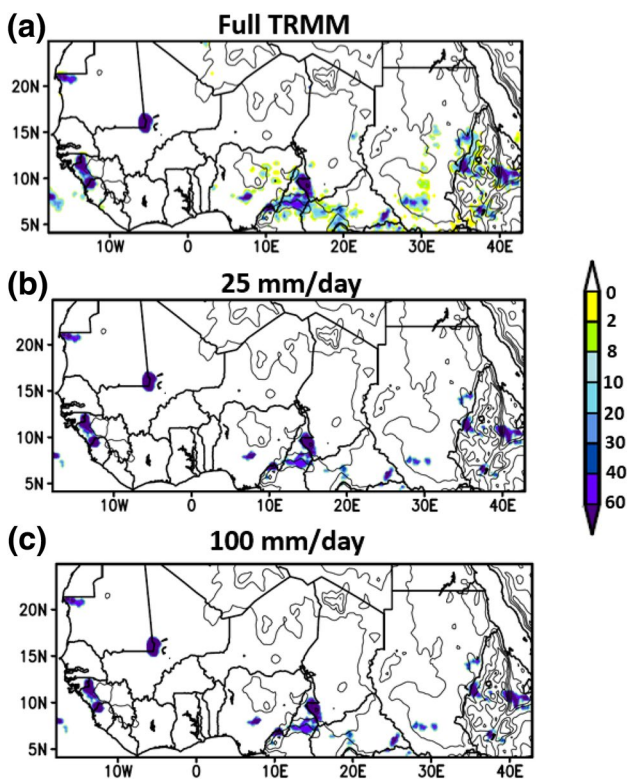


Fig. 3 Spatial distribution of precipitation (mm/day) at 00Z 16 August 2006 for the **a** full TRMM precipitation, **b** T25 precipitation, and **c** T100 precipitation. Thick black contours show country outlines, while the thin black contours show terrain elevation contoured every 500 m from the USGS DEM interpolated to 30-km resolution

full TRMM precipitation at 00Z 16 August 2006, and MCS-related precipitation using the T25 and T100 criteria are shown in Fig. 3b, c, respectively. The T25 criterion produces 26 MCS events over the entire region shown in Fig. 3b, while the T100 criterion (Fig. 3c) produces 12 MCSs, which is 46% of the T25 count. In the full TRMM precipitation (Fig. 3a), heavy rainfall events such as the maximum over northern Cameroon (~15°E, 10°N) are captured by both the T25 and T100 precipitation (Fig. 3b, c). The most notable difference between T25 precipitation and T100 precipitation is the areal extent of the rainfall, and hence the total rainfall associated with MCS activity, as the 25-mm/day threshold yields MCSs with broader areal coverage and higher total precipitation.

4.2 Seasonal variations of MCSs

Figure 4 shows the spatial distribution of the percentage of the full TRMM precipitation delivered by MCSs identified using the T25 threshold for four seasons along with wind vectors (m/s) at 925 hPa from the ERAI reanalysis. Notable differences between JJAS (Fig. 4c) and the other three seasons are the absences of strong zonal and meridional gradients. The percentage of rainfall associated with T25 MCSs during the summer season over most of the analysis region is greater than 80%, with the largest percentages in southwestern Niger (~3°E, 14°N), consistent with other observational studies (Laurent et al. 1998; Mohr et al. 1999; Mohr 2004). Southwesterly monsoon flow intensifies in summer and advances northward across the Sahel to 18°N. The sufficient moist monsoon inflow supports the initiation

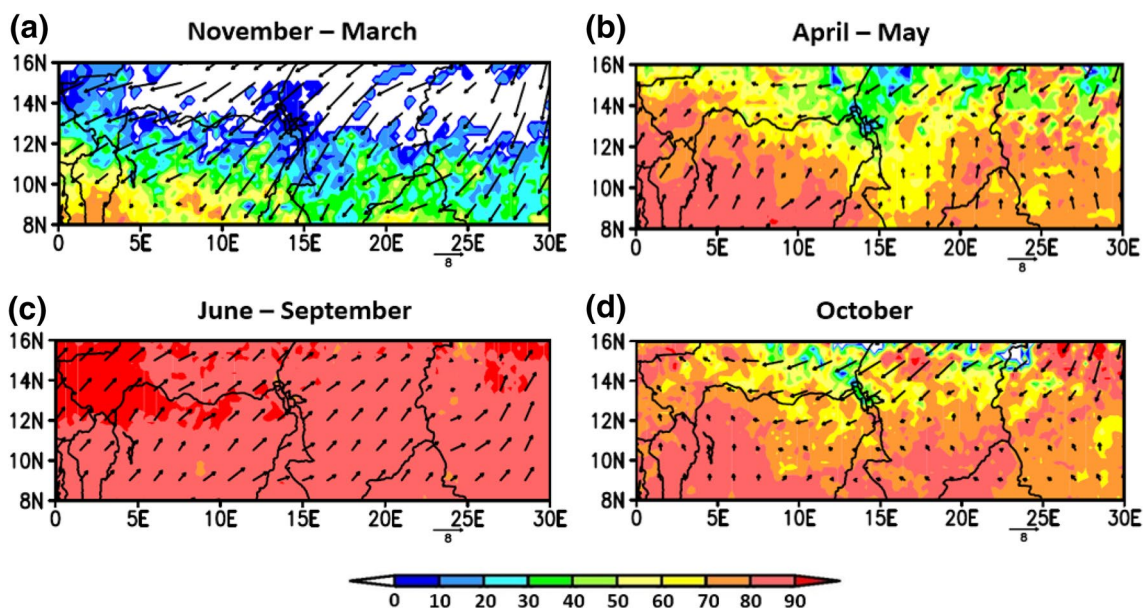


Fig. 4 Percentage of the full TRMM precipitation delivered by T25 precipitation (shaded) for **a** November–March, **b** April–May, **c** June–September, and **d** October. Vectors represent winds (m/s) at 925 hPa from the ERAI reanalysis. Thick black contours show country outlines

and development of organized precipitation systems during the course of the wet season, helping to explain why a large percentage (> 80%) of the rainfall is associated with MCSs in Fig. 4c.

Boreal winter and summer are markedly different in terms of both the spatial patterns and the percentage of rainfall associated with MCSs. During the winter (Fig. 4a), maxima (70%) are located near the Jos Plateau (~7.5°E, 9°N) and over southern Togo and Benin (~3°E, 9°N), which means MCSs play an critical role in rainfall even in winter. Large percentages (greater than 60%) are located farther south (i.e., near 8°N) and west (i.e., west of 10°E), decreasing from 70 to 0% with increasing latitude and, to a lesser extent, longitude. Percentages are lower (30–50%) from southern Chad to southwestern Sudan (16–30°E, 8–11°N). Percentages are below 20% in many areas in southern Niger, central Chad, and western Sudan (6–30°E, 13–16°N), where few rainfall events occur in winter. These spatial distributions are associated with the Harmattan, which is the dry period (i.e., November–March) over Saharan and sub-Saharan northern Africa. The Harmattan is characterized by an intensification of the dry, northeasterly low-level trade winds and increased transport of atmospheric dust over sub-Saharan northern Africa (Mbourou et al. 1997; Schwanghart and Schütt 2008). Low-level climatological convective available potential energy (CAPE) values are less than 100 J/kg in the analysis region, indicating insufficient potential instability in winter. This stability is associated with low atmospheric moisture content over the domain, helping to explain the low frequency of rainfall events and organized MCS systems shown in Fig. 4a.

Unlike the solstitial seasons, differences between boreal spring (AM; Fig. 4b) and fall (Oct; Fig. 4d) distributions are relatively minor. Both seasons have maxima over 80% and meridional gradients of percentages. The largest coherent maxima (80–90%) for both transition seasons occur in Nigeria (3–12°E, 8–12°N), southern Chad (16–22°E, 8–12°N), and southwestern Sudan (24–30°E, 8–12°N), while the lowest values (0–30%) occur to the west of Lake Chad (~14°E, 13.5°N). During these transition seasons, the spatial patterns are associated with the advance (April–May) and retreat (October) of the West African monsoon system (Sultan and Janicot 2003; Issa Lélé and Lamb 2010). During the spring, the persistent Harmattan winds (dry northeasterly trades) relax and retreat north of 14°N over the Sahel while the tropical southerly/southwesterly monsoon flow becomes better established over Nigeria, Benin, and Togo, and, to a lesser extent, southeastern Chad, Central African Republic, and western Sudan. Conversely, in October the tropical southwesterly flow diminishes (Fig. 4d) while the northeasterly trades intensify north of 15°N, ushering in drier air over the Sahel. The Harmattan winds are associated with low CAPE (< 600 J/kg) over the northern part of the domain (13–16°N)

where low percentages of rainfall are associated with MCSs because of the insufficient potential instability. The southerly/southwesterly monsoon flow is associated with moderate instability (CAPE values of 1000–1800 J/kg), contributing to the high percentages (> 80%).

There are some differences between spring and fall. No area has a percentage greater than 90% during spring, but in fall this percentage is exceeded over the Marrah Mountains of western Sudan (26.5°E, 15.5°N) and the Bodélé depression of Chad (17°E, 15°N). The southerly/southwesterly monsoon flow also differs between spring and fall. The monsoon flow is stronger and more westerly in spring. Moisture transport associated with the southwesterly monsoon flow from the Congo Basin may support MCS development in spring. Nicholls and Mohr (2010) indicate that the well-organized MCSs over the Cameroon and the Central African Republic locate well south of the surface baroclinic zone. Additional work is still needed to better understand the regional interactions between the Congo Basin and the West Africa.

Figure 4 highlights the importance of studying MCSs in other seasons besides summer. Although the percentages of MCS rainfall are highest in summer in many areas, there are still regions where very large percentages of the total rainfall come from MCSs in other seasons. From the discussion of Fig. 4, the intensity and position of the Harmattan winds and the tropical southerly/southwesterly monsoon flow are related to the seasonality of MCS activity and their spatial distribution.

Figure 5 shows spatial distributions of the percentage of the full TRMM precipitation delivered by T100 precipitation for the same seasonal averages. The spatial patterns are roughly similar to those using the T25 threshold (Fig. 4) but, of course, the percentages are considerably lower. For example, MCS-related precipitation percentages in winter over the Jos Plateau (~7.5°E, 9°N) range from 30 to 50% for T100 MCSs compared to 70–80% for T25 MCSs. Similarly, during summer, T100 percentages range between 60 and 70%, while they are over 80% for T25 MCSs.

T100 precipitation percentages over the Marrah Mountains (26.5°E, 15.5°N) and Bodélé depression of Chad (17°E, 15°N) in October are close to the T25 precipitation percentages in these regions, ranging from 70 to 90% and 50–80%, respectively. This indicates that the majority of the rainfall in these regions is associated with very intense systems. Similarly strong T100 activity is not apparent in the April–May average (Fig. 5b), although spring and fall are both transition seasons. However, an examination of April percentages shows high T100 precipitation percentages of 70% over (29°E, 14.5°N), on the east of the Marrah Mountains. In May, percentages of 70% occur near 27°E and 15.5°N, north of the Marrah Mountains, and at 14°E and 15.5°N near the Bodélé depression. These are lower

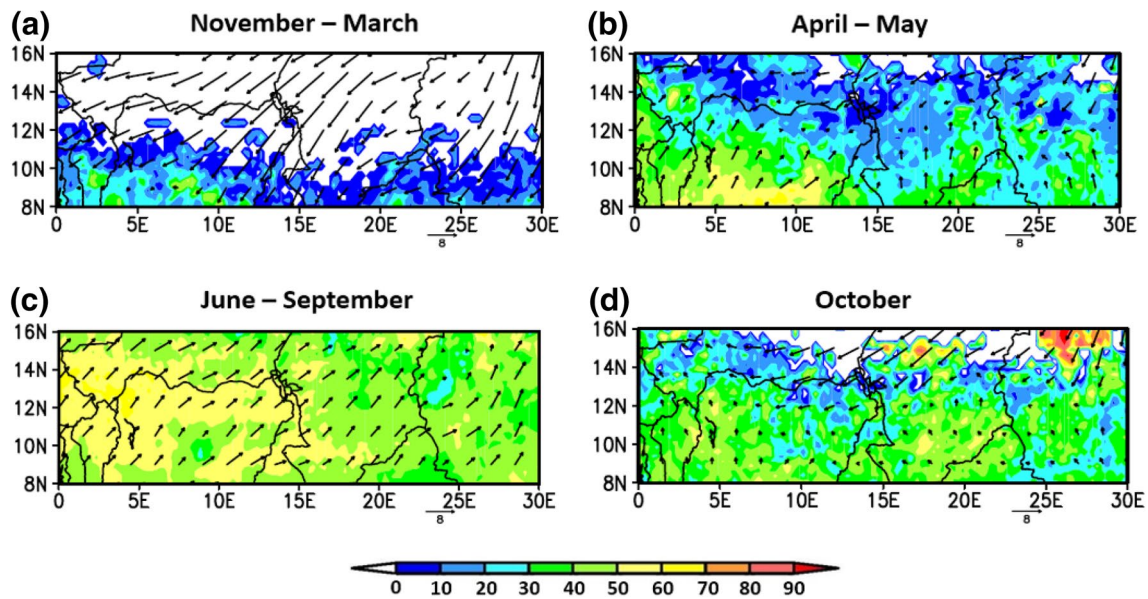


Fig. 5 Percentage of the full TRMM precipitation delivered by T100 precipitation (shaded) for **a** November–March, **b** April–May, **c** June–September, and **d** October. Vectors represent winds (m/s) at 925 hPa from the ERAI reanalysis. Thick black contours show country outlines

than the maxima of 90% in October. The orography of the Marrah Mountains may play an influential role in helping to trigger/organize convection, while surface heating and/or the surrounding topography may be influential over the Bodélé depression.

4.3 Diurnal cycles

Figures 4 and 5 show that the percentage of precipitation related to MCS activity has a strong meridional gradient in the winter, spring, and fall. Because of this meridional dependence, we examine the diurnal cycle every 2° of latitude over the 0–30°E domain shown in Fig. 1a.

The black lines in Fig. 6 indicate the percentage of the full TRMM precipitation that falls in each 3-h time period. The percentage that is delivered by T25 and T100 MCSs is indicated by the red and green lines, respectively. Figure 6a–d show percentages for the four seasons defined above in a northern area (0–30°E, 14–16°N), and Fig. 6e–h show percentages in each season for a southern area (0–30°E, 10–12°N). Northern and southern areas are selected to represent the northern and southern parts of our domain.

In general, in all seasons and locations, the percentages of T25 and T100 precipitation have diurnal cycles that are similar to the full TRMM precipitation. T25 and T100 precipitation contribute to the full TRMM rainfall throughout the year, but the contribution is greatest in summer and smallest in winter. In winter, the contribution of T25 MCSs to the full TRMM precipitation is 0–30% in the north and ~60% in the south. In both transition seasons, T25 precipitation contributes 65–80% of the full TRMM

rainfall. In summer, the percentages range from 80 to 93% for the T25 metric, and the contribution of T100 MCSs is around half of the T25 MCS contribution.

To better understand the diurnal cycle of MCSs, we examine the diurnal cycles of MCS count, size, and intensity. Does the daily precipitation peak occur because more MCSs occur at that time, or is it because MCSs are larger and/or stronger? Results are shown for T25 MCSs, but the results are similar for T100 MCSs.

Figure 7 displays the climatological diurnal cycles of the T25 MCS count over the northern and southern regions in each season. The climatological T25 MCS count is calculated by averaging the number of T25 MCSs over 1998–2014 at each 3-h time period and then averaged over northern and southern regions. The count of T25 MCSs has an afternoon maximum, at 15Z or 18Z, in all four seasons in both regions. MCS numbers increase from 06Z or 09Z, reach a maximum in the afternoon (15Z or 18Z), and then decrease until the morning of the following day. In general, the diurnal cycle of T25 MCS sizes coincides with the diurnal cycle of T25 precipitation shown in Fig. 6. The count of MCSs is large when rainfall rates are high, showing that the count of MCSs is one of the reasons for the diurnal precipitation peaks. The count of MCSs is lowest in winter and highest in summer. Spring and fall have similar diurnal cycles of MCS counts.

There is a marked difference in MCS counts between the two domains. The count in the northern region is only about 16% of the count in the southern region in spring and fall (Fig. 7b, d), but it is 30–40% during the wet season

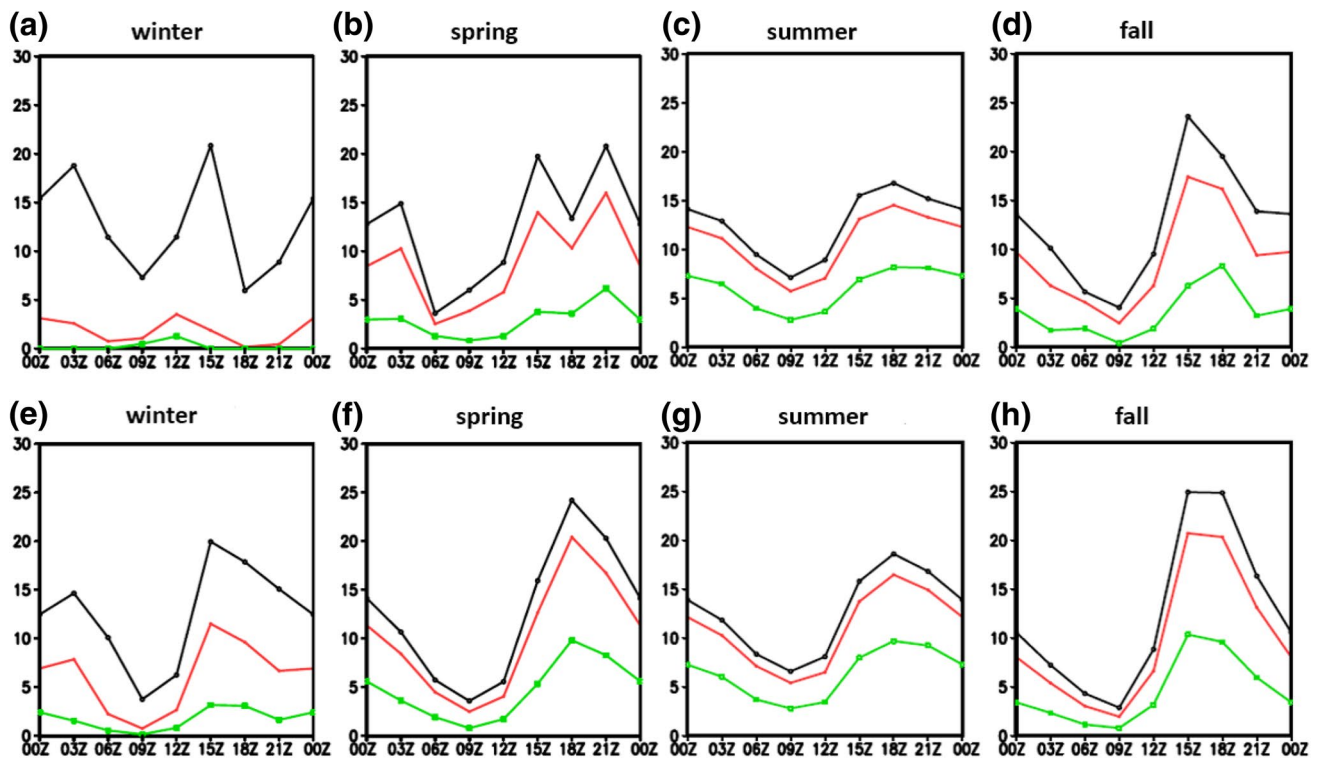


Fig. 6 Percentage of full TRMM precipitation (black), T25 precipitation (red) and T100 precipitation (green) at each time period in the sum of full TRMM precipitation at all time periods for November–March (a, e), April–May (b, f), June–September (c, g) and October

(d, h) over northern (a–d) and southern (e–h) areas. Northern area and southern area are selected as (0–30°E, 14–16°N) and (0–30°E, 10–12°N) separately

(Fig. 7c). The count in winter (Fig. 7a) is so low that we cannot obtain useful information.

The diurnal cycles of MCS rainfall intensity (i.e., maximum rainfall rate) and size are also examined (not shown). The results are similar to those for the diurnal cycle of MCS count shown in Fig. 7, indicating that the size, intensity and number of T25 MCSs all contribute to the diurnal cycle of T25 precipitation. These three attributes are closely linked in the dynamics of MCSs, and they are also associated with the seasonal and meridional variability of MCSs.

Zhang et al. (2016a) examined the climatological diurnal cycle of rainfall in summer over part of our analysis region, and found that averaging over large regions can obscure the nature of regional diurnal cycles of precipitation. To avoid such misunderstanding, we examine the climatological diurnal cycle of rainfall area-averaged over $1^\circ \times 1^\circ$ grid boxes from 0° to 30° E and 8° N to 16° N for the four seasons, similar to Fig. 4 in Zhang et al. (2016a). Summer and fall are shown in Fig. 8a, b respectively. Distributions for spring are similar to fall.

We classify the precipitation diurnal cycles into the following three categories: single afternoon peak, continuous afternoon peak, and nocturnal peak. They are represented

by the different colors in Fig. 8. The features and criteria of three categories are summarized as follows:

- Single afternoon peak (pink): maximum rainfall occurs in the afternoon (15Z or 18Z). The rainfall decreases by more than 50% from the peak hour to midnight (00Z).
- Continuous afternoon peak (green): maximum rainfall occurs in the afternoon (15Z or 18Z), and the rainfall rate decreases by less than 50% from the peak hour to midnight (00Z). This can indicate that the rainfall peak persists until midnight with a flat or slightly declining slope from afternoon to the midnight. One special case is also considered as a continuous afternoon peak. The maximum rainfall occurs at night but afternoon rainfall is more than 90% of the maximum rainfall, indicating the rainfall peak starts from afternoon and persists to midnight.
- Nocturnal peak (blue): maximum rainfall occurs at 21Z, 00Z, or 03Z without a high (> 90% of the maximum rainfall) rainfall rate in the afternoon.

These criteria provide an overall assessment of the geographical distribution of the diurnal cycle types, but the classification of the individual 1° boxes is sensitive to the

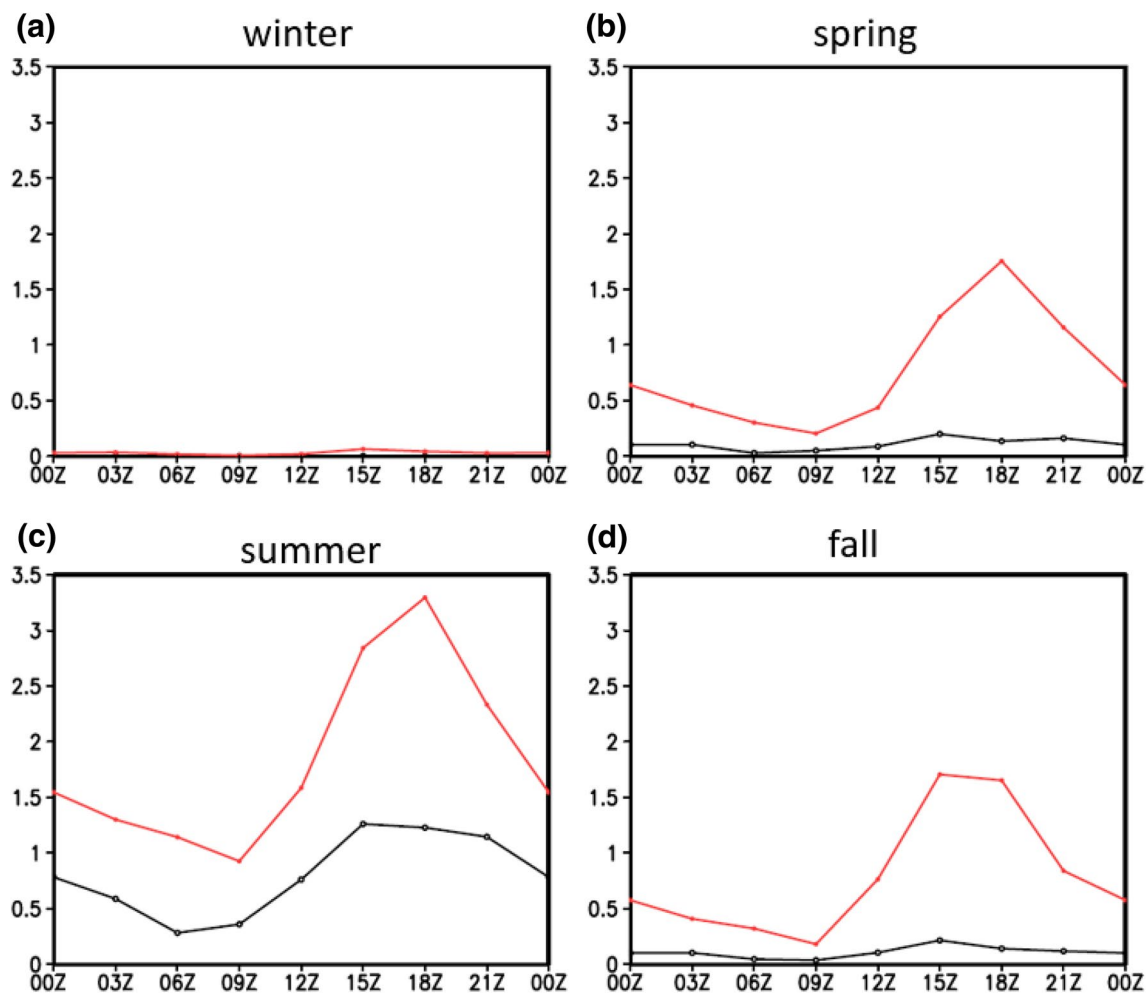


Fig. 7 The climatological diurnal cycle of the T25 MCS count over the northern (0–30°E, 14–16°N; black) and southern (0–30°E, 10–12°N; red) domains for **a** November–March, **b** April–May, **c** June–September, and **d** October

specification of the criteria because adjacent locations have similar diurnal cycles at this fine-scale resolution.

Some of the boxes have very low rainfall rates and, as a result, diurnal cycles that are barely discernible. Examples include rainfall at (9–17°E, 16°N) in Fig. 8a and to the north of 12°N in Fig. 8b. We do not consider these regions, and to filter them out 1° boxes with maximum rainfall rates below 1 mm/day are neglected. Table 2 shows numbers and percentages of the remaining 1° boxes with single afternoon peaks, continuous afternoon peaks, and nocturnal rainfall peaks.

In spring and fall, diurnal cycles with single afternoon peaks are most common, occurring in more than 45% of the 1° boxes, while continuous afternoon and nocturnal peaks are more rare (11 and 16%, respectively). In contrast, regions with continuous afternoon peaks rise to 32% in summer, and they are more common than regions with single afternoon peaks (24%). However, regions with nocturnal peaks are the most common in summer, occurring in 41.5% of the

1° boxes. This clearly shows that local diurnal precipitation cycles vary seasonally.

Zhang et al. (2016a, b) found that nocturnal rainfall peaks occur primarily in two regions (2°E–5°E; 9°N–11.5°N and 2°E–5°E; 13.5°N–16.5°N) in summer, which agrees with Fig. 8a, and that they are associated with propagating systems downstream of topography or afternoon precipitation maxima. A number of previous studies (Shinoda et al. 1999; Laing et al. 2008) have shown that nocturnal peaks are due to propagating systems that originate over topography or in association with the inter-tropical front downstream of regions with gradually sloping terrain (Vizy and Cook 2017).

Here we focus on the physical mechanisms responsible for the two types of afternoon peaks, and the seasonality of the diurnal cycles. We choose two regions for closer analysis, denoted by the boxes in Fig. 8a. One region (27–30°E, 8–10°N), which is referred to as SP, is dominated by summertime single afternoon rainfall peaks, while the other

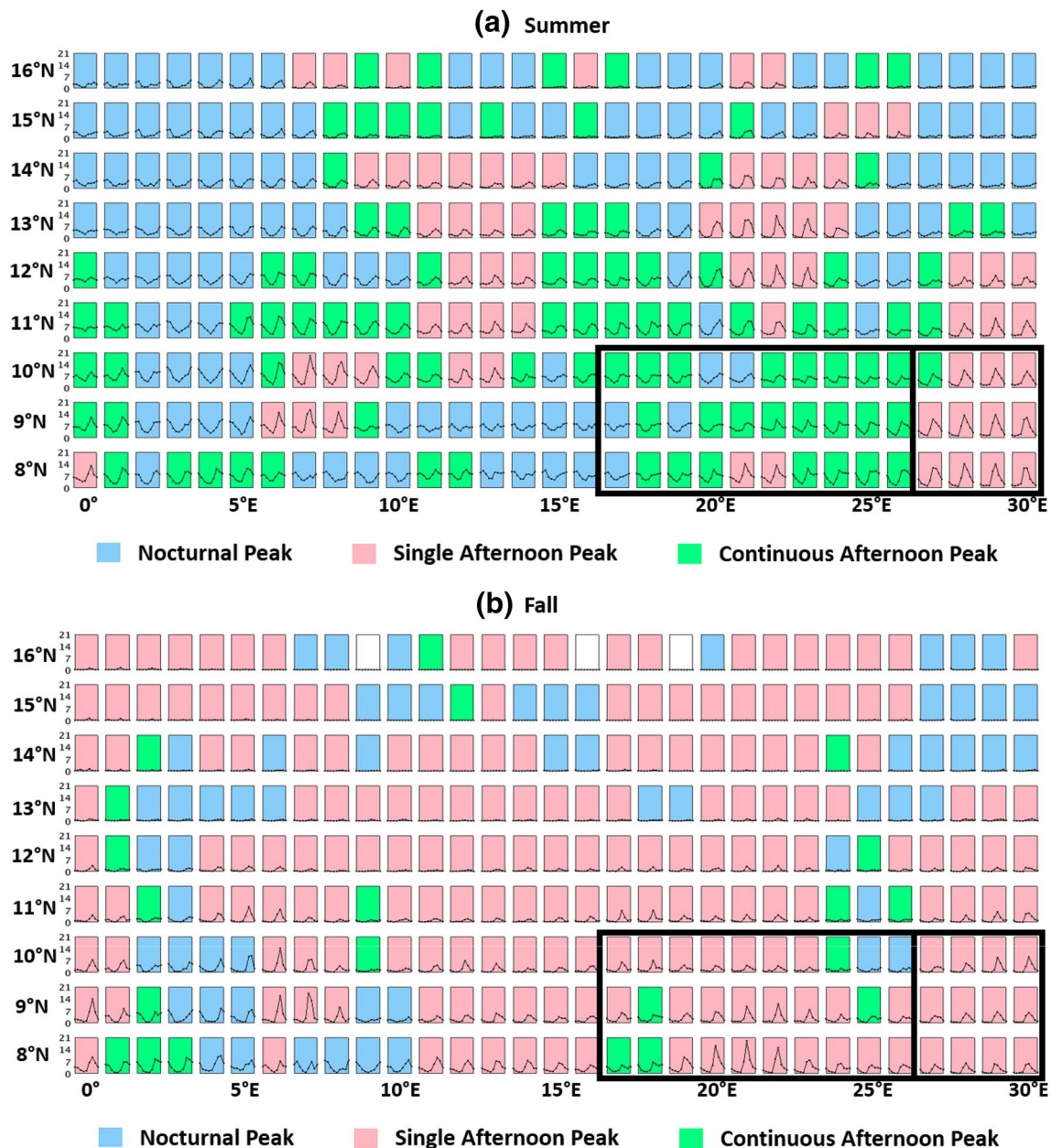


Fig. 8 Diurnal cycle of climatological **a** summer and **b** fall rainfall (mm/day) area-averaged for $1^\circ \times 1^\circ$ grid boxes over the region bounded by 0° – 30° E, 8° N– 16° N. The x-axis of each panel ranges from 00 Z to 24 Z at 3 h intervals. Boxes denote region with predomi-

nant single afternoon peak (17 – 26° E, 8 – 10° N) and predominant continuous afternoon peak (17 – 26° E, 8 – 10° N). Grid boxes with nocturnal rainfall peaks, single afternoon peaks, and continuous afternoon peaks are shaded in blue, pink, and green respectively

region (17 – 26° E, 8 – 10° N), referred to as CP, is dominated by summertime continuous afternoon peaks. They are located in the southern part of the analysis region to maximize the number of seasons with rainfall. Although the SP and CP regions are not completely uniform in terms of their diurnal cycles chosen by the above criteria, the diurnal cycles in the analysis regions are similar. In the analysis, the dependence of the results on the choice of averaging regions is tested.

Both the SP and the CP regions have summertime afternoon rainfall peaks, but their persistence is different. We explore the reason for this difference in persistence by comparing the vertical profiles of moist static energy (MSE) over the two domains. MSE measures atmospheric stability, and it is defined as the sum of the sensible, latent, and geopotential heat contents of a parcel according to

$$MSE = c_p T + Lq + gz \quad (1)$$

Table 2 Numbers and percentages of 1° boxes with single afternoon peaks, continuous afternoon peaks, and nocturnal rainfall peaks exceeding 1 mm/day

Season	Single afternoon peak	Continuous afternoon peak	Nocturnal peak
Winter	3 (0.7%)	0 (0%)	2 (0.7%)
Spring	85 (50%)	18 (11%)	45 (16%)
Summer	68 (24%)	90 (32%)	116 (41.5%)
Fall	127 (45.5%)	15 (5%)	25 (8%)

In (1), c_p is the specific heat of air at constant pressure, T is the air temperature, L is the latent heat of water vaporization, q is the specific humidity, g is gravitational acceleration, and z is the geopotential height. MSE profiles can discriminate the individual roles of temperature and moisture in generating convective instability.

Figure 9a shows profiles of MSE at 18Z from the 6-hourly ERAI reanalysis averaged over summer rainy days for the SP (solid line) and CP (dashed line) regions. Rainy days are selected as dates with daily-averaged rainfall rates of 3 mm/day or greater in the TRMM 3B42 time series. We tested the rainfall threshold from 0 to 5 mm/day. The MSE profiles are not sensitive for the rainfall threshold. 18Z is chosen since it is the time when the single afternoon peaks start to dissipate while the continuous afternoon peaks persist. Later time periods, such as 00Z, yield similar results, and the results are also not sensitive to the choice of the rainfall threshold. Figure 9b, c display the Lq and c_pT components of MSE, respectively.

The total MSE profiles, and each component, are similar in the two regions. The gz component of MSE (not shown) is the same over the two domains as well. This indicates that locally-generated instabilities are not responsible for the differences in the diurnal cycle.

Since the differences between the SP and CP diurnal cycles are not explained by differences in locally-generated instability, we hypothesize that they are related to propagating systems. Figure 10a–d show climatological Hovmöller diagrams of the TRMM 3-hourly rainfall climatology averaged from 8°N–10°N for typical weeks in winter, spring, summer, and fall, respectively. The locations of the CP and SP regions in Fig. 8 are indicated in Fig. 10c. In winter (Fig. 10a), the number of rainfall events and the volumetric rainfall rates are small. A few rain-producing systems are generated around the Jos Plateau (~7.5°E) and the Ethiopian Highlands (35–40°E), showing the influence of topography in initiating MCSs (Hodges and Thorncroft 1997; Mohr et al. 1999; Mohr 2004, and; Fink et al. 2006).

A relationship to topography is also evident in the other seasons (Fig. 10b–d), as rainfall systems form over the Ethiopian Highlands (35–40°E, 8–10°N) in the afternoon of each day in the climatology from May 11 to October 14. Two types of rainfall systems influence the diurnal cycle of rainfall over the analysis region. One is long-lived systems originating over the Ethiopian Highlands, and the other is more locally-generated rainfall systems. We consider each type and its contribution to the seasonality of the diurnal cycle.

In spring (Fig. 10b), systems generated over the Ethiopian Highlands persist for 12–15 h and they have propagation

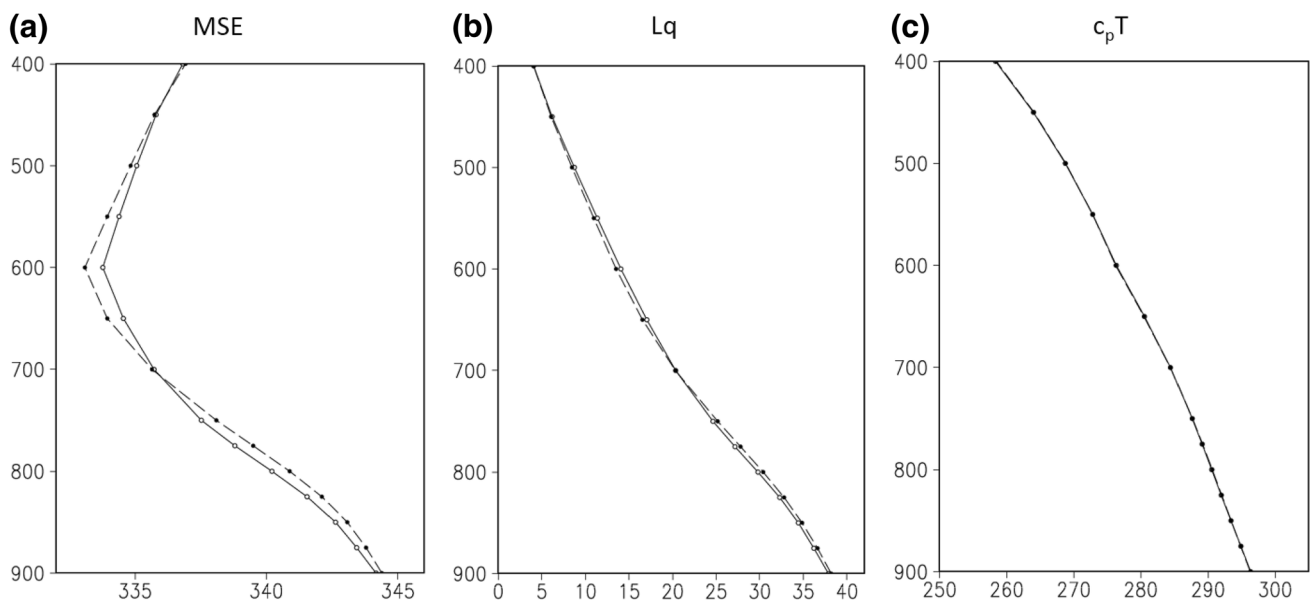


Fig. 9 Profiles of **a** the MSE, **b** Lq , and **c** c_pT at 18Z for summer rainy days over the SP (solid line) and CP regions (dashed line) from the ERAI reanalysis. Units are 10^6 J/kg

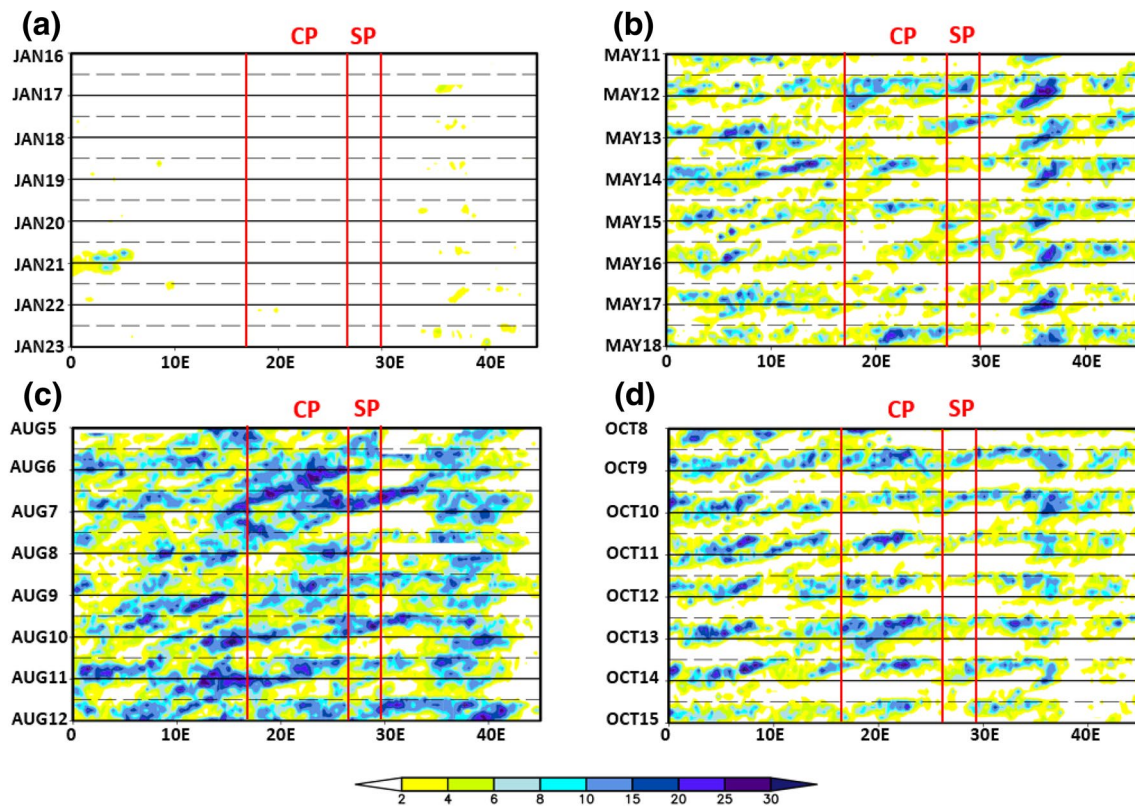


Fig. 10 Climatological Hovmöller diagrams of TRMM 3-hourly rainfall (mm/day) averaged from 8°N–10°N for **a** January 16–22, **b** May 11–17, **c** August 5–11, and **d** October 8–14. Red lines denote the

boundaries of the SP (27–30°E, 8–10°N) and CP (17–26°E, 8–10°N) domains. Solid black lines denote 00Z while dashed black lines denote 12Z at each day

speeds of 5 m/s on average. The propagations of these systems start from 38°E and end at 34°E. They do not propagate to the analysis regions (east of 30°E) so they do not influence the diurnal cycle of rainfall in the spring. One reason that limits the duration of propagation may be insufficient moisture in spring compared with summer in association with the position and intensity of the monsoon flow. Within the analysis domain, most springtime MCSs start at noon and dissipate at night with lifetimes of around 9 h. These MCSs are the sources of the single afternoon peaks, which are dominant in Table 2. For instance, one system initiates at 12Z on May 13 at 15°E and propagates westward to 11°E at 21Z. On the other hand, some MCSs have a lifetime longer than 12 h, such as the MCS initiated at 12Z on May 11 at 24°E. These MCSs generate rainfall at night, and they are the source of the continuous afternoon peaks and nocturnal peaks. In spring, MCSs with long lifetimes are in a minority compared with these short-lived MCSs.

In summer, both the distance and duration of MCS propagation increases. The speed of propagation in summer is around 15 m/s, which agrees with past studies (Shinoda et al. 1999; Laing et al. 2011). As seen in Fig. 10c, the rainfall systems that form over the Ethiopian Highlands (35–40°E,

8–10°N) persist for longer than 12 h, and 4% of these rainfall systems impact the analysis domains. For example, an MCS forms over the Ethiopian Highlands at 37°E in the late evening of August 5 and persists longer than one day. It moves westward 10° of longitude and contributes to the rainfall in the SP region. Due to the distance between the SP region and the Ethiopian Highlands, MCS systems from the Ethiopian Highlands arrive the SP region after 12Z and bring afternoon rainfall. Differences in MCS characteristics in spring and summer may be related to differences in the downstream monsoon inflow. For example, the monsoon inflow and the cold-pool outflow from MCSs can generate low-level convergence, helping to trigger new cells and lengthen MCS lifetimes (Marsham et al. 2013a; Garcia-Carreras et al. 2013; Provod et al. 2016). As shown in Fig. 4, the monsoon inflow is strongest and advances northward across the Sahel to 18°N in summer, supporting summer MCS development and maintenance.

In the SP region, MCSs normally form at 12Z and propagate westward after the initiations. According to the speed of propagation, the MCSs emerge from the western boundary of the SP region (27°E) and enter the CP region around midnight. Propagating rainfall systems from the SP region

bring nocturnal rainfall to the CP region. In addition to propagating systems, MCSs are locally generated over the CP region. Bongo Massif (22°E, 8°N) of northeastern Central African Republic is likely important for locally generated convections. Rainfall over the CP region combines locally generated MCSs' rainfall in the afternoon and propagating systems' rainfall at night. Thus, the afternoon peaks in the CP region do not dissipate immediately but persist to midnight. In other words, the continuous afternoon peak combines rainfall from two individual system types—one locally-generated and one propagating. Continuous afternoon peaks shown in Fig. 8 are unlikely to occur without propagating systems.

The situation in fall is similar to spring, as shown in Fig. 10d. The speed of MCS propagation, 10–12 m/s, is slower than in summer, and the typical MCS lifetime is less than a half day compared with 2 days in summer. Most MCSs develop at around 12Z and dissipate before midnight, forming the single afternoon rainfall peak. A few MCSs live longer than 12 h bringing continuous afternoon peaks and nocturnal peaks. The number of long-lived MCSs is low causing the low percentages of continuous afternoon peaks (5%) and nocturnal peaks (8%) in Table 2.

Past studies (Tuttle and Carbone 2004; Miyakawa and Satomura 2006) show that MCSs propagate not only zonally but also meridionally. Figure 10 addresses only zonal propagation. Figure 11a, b show climatological Hovmöller diagrams of the TRMM 3-hourly rainfall averaged over 20–23°E for typical weeks in spring and summer, respectively. We examined other longitudes in our analysis domain, such as 27–30°E. Similar results was found. In spring (Fig. 11a), the MCSs also have a southward propagation component. For example, the MCS that formed at noon on May 11 propagates southward from 10°N to 5°N over 12 h. Combing this southward component with the westward propagation shown in Fig. 10, the propagation direction tends to be southwestward in spring. The MCSs propagate across the southern boundary (8°N) of the analysis domain, which is shown as the red line in Fig. 11a.

In contrast to spring, MCSs do not have a strong southward propagation component in summer (Fig. 11b). This result reveals that the direction of propagation also changes seasonally. The direction of propagation influences the location of nocturnal precipitation and contributes to the pattern of the diurnal cycle. This difference in the direction of propagation is likely to be related to the wind at 600 hPa, where the easterlies are stronger in summer than in spring, especially over 11–16°N. There is also a stronger northerly component of the large-scale flow in spring. The seasonal variation of propagation direction corresponds with changes in the direction of the large-scale background flow.

Although the MSE profiles in Fig. 9a do not show obvious differences between the SP and CP domains, MSE

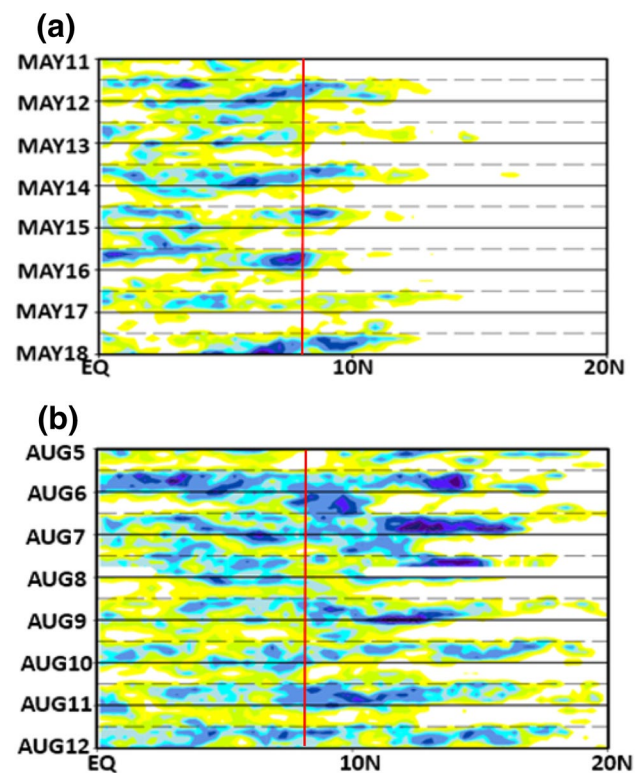


Fig. 11 Climatological Hovmöller diagrams of TRMM 3-hourly rainfall (mm/day) averaged between 20°E–23°E for **a** May 11–17 and **b** August 5–11 from 1998 to 2014. Solid black lines denote 00Z while dashed black lines denote 12Z at each day. Red lines denote the southern boundaries (8°N) of CP (17–26°E, 8–10°N) domain

profiles are useful for understanding the seasonality of MCS lifetimes and propagation features. Figure 12a–c show the area-averaged (17–30°E, 8–10°N) ERAI vertical profiles at 18Z of total MSE, L_q , and $c_p T$, respectively, for each of the four seasons. The averaging region (17–30°E, 8–10°N) includes both CP and SP regions. The smaller subsets of the region, such as (20–25°E, 8–10°N), are examined for averaging to reduce the risk of obscuring results by averaging over too large of a region. Results of smaller subsets are similar with Fig. 12. Similar with Fig. 9, 18Z is chosen because this is the critical time when the afternoon peak either dissipates or persists to midnight. Table 3 shows the 600 hPa–900 hPa difference of MSE, L_q , and $c_p T$ for the winter, spring, summer and fall in Fig. 12 to provide an estimate of the vertical profile slopes in Fig. 12. The variations of the geopotential term (gz ; not shown) are found to be not relevant.

The MSE profile in winter (Fig. 12a) is nearly neutral from 600 to 900 hPa. MSE profiles in spring, summer, and fall indicate a decrease in MSE with increasing height from the surface, indicating the atmosphere is unstable and the potential for convection has increased. Combining Fig. 12b and Table 3 indicates that the contribution to instability (as measured by MSE) is largest from the

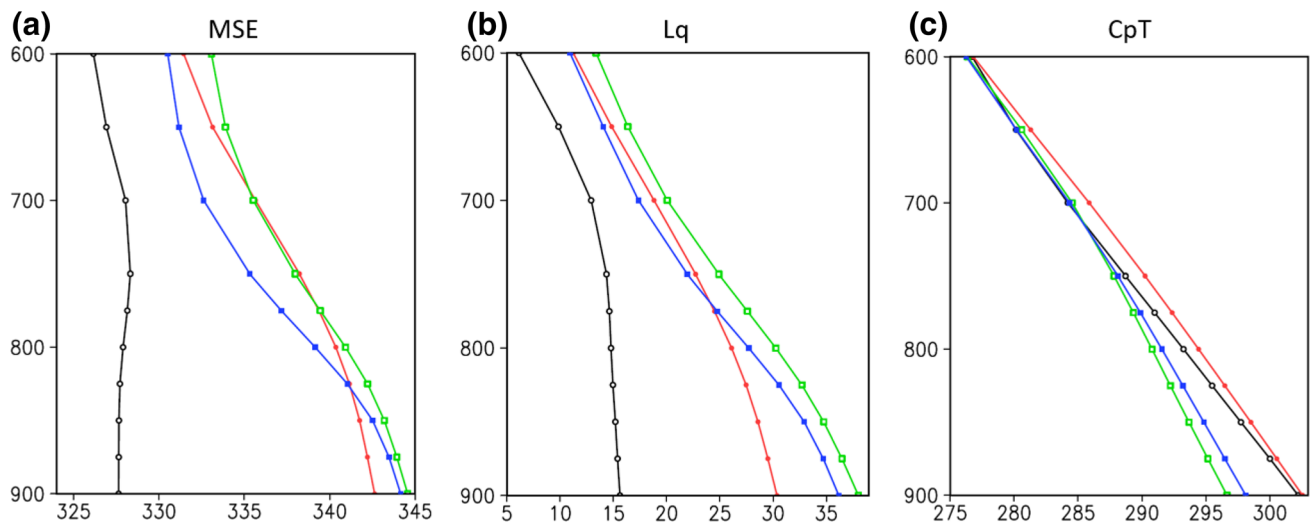


Fig. 12 Profiles of average ERA-Interim **a** total MSE, **b** Lq , and **c** $c_p T$ at 18Z in winter (black), spring (red), summer (green) and fall (blue) over (17–30°E, 8–10°N). Units are 10^6 J/kg

Table 3 The differences of MSE, Lq and $c_p T$ at 600 hPa and 900 hPa in winter, spring, summer and fall in Fig. 12. Units are 10^6 J/kg

	MSE	Lq	$c_p T$
Winter (black)	– 1.05	– 8.76	– 25.796
Spring (red)	– 10.98	– 18.68	– 26.03
Summer (green)	– 11.69	– 24.94	– 20.17
Fall (blue)	– 13.26	– 24.52	– 22.18

moisture component, Lq , in the summer and fall; this contribution is minimal in winter. The moist southwesterly monsoon flow advances northward in spring and retreats southward in fall, providing more moisture to support long-lived MCSs in the warm season. Long-lived propagating rainfall systems bring nocturnal rainfall and form continuous afternoon and nocturnal rainfall peaks. In contrast, the dry northeasterly air of the Harmattan develops in the fall and weakens in spring, inhibiting MCS longevity.

In contrast, the thermal component of MSE, $c_p T$, is more important for producing low-level instability during winter and spring, and it is less influential during the summer. Higher temperatures near the surface promote rising motion, increasing atmospheric instability and promoting MCS formation. Temperature and moisture fluxes within the planetary boundary layer can affect CAPE, atmospheric instability, and associated rainfall events (Alapaty et al. 1997; Pielke 2001; Holt et al. 2006). Despite the similarity of the transition seasons, $c_p T$ is more influential in determining instability during the spring, while Lq is more influential during boreal autumn.

5 Conclusions

Heavy rainfall events over sub-Saharan northern Africa are usually related to MCSs. While previous studies diagnose the role of MCSs in total rainfall, they consider only individual, or a small number, of summer seasons. We evaluate the role of MCSs in the total rainfall distribution as a function of season from a climatological perspective over sub-Saharan northern Africa and examine how the diurnal cycle of rainfall changes with season.

MCSs are defined here as events that have a contiguous spatial area encompassed by the 25 mm/day rainfall contour that is greater than 2000 km² in the 3-hourly TRMM 3B42V7 rainfall estimates (Huffman et al. 2007). Another rainfall threshold, 100 mm/day, is examined to understand the features of intense MCSs. Our selections of MCSs with the rainfall thresholds, 25 mm/day and 100 mm/day, are referred to as T25 and T100, respectively.

The conclusions are summarized as follows:

- MCSs identified from TRMM 3B42V7 observations using 2 rainfall intensity criteria (T25 and T100) show similar spatial distributions, the MCS counts are different. The most notable difference between T25 precipitation and T100 precipitation is the areal extent of the rainfall, and hence the total rainfall associated with MCS activity.
- The percentage of the full TRMM precipitation delivered by T25 MCSs varies meridionally from 0 to 80% over sub-Saharan northern Africa in the spring, fall and winter, while the percentages are homogenous in summer (> 80%). The intense rainfall events captured in the T100 MCS count are mostly similar. However, there is a

maximum in the T100 rainfall during the transient seasons over the Marrah Mountains and Bodélé depression of Chad that does not occur in the T25 rainfall. This indicates that the majority of the rainfall that falls over these areas is associated with very intense systems.

- Diurnal cycles of MCS-related precipitation are coincident with the diurnal cycles of the full TRMM rainfall in all four seasons. The contribution of T25 MCSs to the full TRMM precipitation is 0–60% in winter and 80–93% in summer. In both transition seasons, T25 precipitation contributes 65–80% of the full TRMM rainfall. The contribution of T100 MCSs is around half of the T25 MCS contribution year around. The diurnal cycles of MCS size, count and intensity are the same as the diurnal cycle of rainfall.
- The diurnal cycles can be classified into three categories: single afternoon peak, continuous afternoon peak, and nocturnal peak. The diurnal cycle types vary seasonally. Diurnal cycles with single afternoon peaks are most common in spring and fall, with over 45% of our analysis region experiencing a single afternoon peak in transition seasons. Continuous afternoon peaks are more common than single afternoon peaks in summer, and nocturnal peaks are the most common in summer.
- The continuous afternoon peak combines rainfall from two system types – one locally-generated and one propagating. The seasonality of the diurnal cycle is related to the seasonality of MCS lifetimes, propagation speeds and directions. In dry seasons, most MCSs start at noon and dissipate with short lifetimes and low propagation speeds, so they cannot generate the nighttime rainfall that leads to continuous afternoon peaks and nocturnal peaks. In wet seasons, MCS lifetimes are longer and the speeds of propagations are higher. Long-lived westward propagating MCSs contribute to the continuous afternoon peaks and the nocturnal peaks.
- Moisture static energy (MSE) profiles cannot explain the distribution of different types of diurnal cycles within a season, but they do help explain seasonality. An MSE analysis shows the atmosphere is unstable in spring, summer and fall, increasing the potential for convection. The moisture component of MSE, Lq , provides the largest contribution to the instability in the summer and fall. Seasonal variations of the southwesterly monsoon flow and dry northeasterly air of the Harmattan influence the moisture component. In contrast, the temperature component, $c_p T$, is more influential in generating instability during the winter and spring seasons.

This work indicates that an understanding of MCS formation and propagation characteristics is essential for understanding both the diurnal cycles of rainfall and the seasonality of rainfall over northern Africa. Extending studies of

MCSs beyond summer is necessary to better understand African weather and climate, contributing to an improved ability to predict extreme rainfall events over Africa.

Acknowledgements Support from NSF Award #1444505 is gratefully acknowledged. Dr. Gang Zhang provided much appreciated assistance as well.

References

- Alapaty K, Pleim JE, Raman S, Niyogi DS, Byun DW (1997) Simulation of atmospheric boundary layer processes using local-and non-local-closure schemes. *J Appl Meteorol* 36(3):214–233. [https://doi.org/10.1175/1520-0450\(1997\)036<0214:SOABLP>2.0.CO;2](https://doi.org/10.1175/1520-0450(1997)036<0214:SOABLP>2.0.CO;2)
- Birch CE, Marsham JH, Parker DJ, Taylor CM (2014a) The scale dependence and structure of convergence fields preceding the initiation of deep convection. *Geophys Res Lett* 41:4769–4776. <https://doi.org/10.1002/2014GL060493>
- Birch CE, Parker DJ, Marsham JH, Copsey D, Garcia-Carreras L (2014b) A seamless assessment of the role of convection in the water cycle of the West African Monsoon. *J Geophys Res* 119:2890–2912. <https://doi.org/10.1002/2013JD020887>
- Burpee RW (1972) The origin and structure of easterly waves in the lower troposphere of North Africa. *J Atmos Sci* 29:77–90. [https://doi.org/10.1175/1520-0469\(1972\)029<0077:TOASOE>2.0.CO;2](https://doi.org/10.1175/1520-0469(1972)029<0077:TOASOE>2.0.CO;2)
- Cook KH (1999) Generation of the African Easterly jet and its role in determining West African precipitation. *J Clim* 12:1165–1184. [https://doi.org/10.1175/1520-0442\(1999\)012<1165:GOTAEJ>2.0.CO;2](https://doi.org/10.1175/1520-0442(1999)012<1165:GOTAEJ>2.0.CO;2)
- Crétat J, Vizy EK, Cook KH (2015) The relationship between African easterly waves and daily rainfall over West Africa. Observations and regional climate simulations. *Clim Dyn* 44:385–404. <https://doi.org/10.1007/s00382-014-2120-x>
- Dee DP, Uppala SM, Simmons AJ et al (2011) The ERA-Interim reanalysis: configuration and performance of the data assimilation system. *Q J Roy Meteorol Soc* 137:553–597. <https://doi.org/10.1002/qj.828>
- Diedhiou A, Janicot S, Viltard A, de Félise P, Laurent H (1999) Easterly wave regimes and associated convection over West Africa and the tropical Atlantic: results from the NCEP/NCAR and ECMWF reanalyses. *Clim Dyn* 15:795–822. <https://doi.org/10.1007/s003820050316>
- Duvel J-P (1989) Convection over tropical Africa and the Atlantic Ocean during northern summer. Part I: interannual and diurnal variations. *Mon Weather Rev* 117:2782–2799. [https://doi.org/10.1175/1520-0493\(1989\)117<2782:COTAAT>2.0.CO;2](https://doi.org/10.1175/1520-0493(1989)117<2782:COTAAT>2.0.CO;2)
- Eldridge RH (1957) A synoptic study of West African disturbance lines. *Q J Roy Meteorol Soc* 83:303–314. <https://doi.org/10.1002/qj.49708335704>
- Fink AH, Reiner A (2003) Spatiotemporal variability of the relation between African easterly waves and West African squall lines in 1998 and 1999. *J Geophys Res* 108:4332. <https://doi.org/10.1029/2002JD002816>
- Fink AH, Vincent DG, Ermert V (2006) Rainfall types in the West African Sudanian zone during the summer monsoon 2002. *Mon Weather Rev* 134:2143–2164. <https://doi.org/10.1175/MWR3182.1>
- Fortune M (1980) Properties of African squall lines inferred from time-lapse satellite imagery. *Mon Weather Rev* 108(2):153–168. [https://doi.org/10.1175/1520-0493\(1980\)108<0153:POASLI>2.0.CO;2](https://doi.org/10.1175/1520-0493(1980)108<0153:POASLI>2.0.CO;2)
- Garcia-Carreras L, Marsham JH, Parker DJ, Bain CL, Milton S, Saci A, Salah-Ferroudj M, Ouchene B, Washington R (2013) The impact of convective cold pool outflows on model biases in the Sahara.

- Geophys Res Lett 40(8):1647–1652. <https://doi.org/10.1002/grl.50239>
- Gaye A, Viltard A, De Felice P (2005) Squall lines and rainfall over Western Africa during summer 1986 and 87. *Meteorol Atmos Phys* 90(3):215–224. <https://doi.org/10.1007/s00703-005-0116-0>
- Hodges KI, Thorncroft CD (1997) Distribution and statistics of African mesoscale convective weather systems based on ISCCP METEOSAT imagery. *Mon Weather Rev* 125:2821–2837. [https://doi.org/10.1175/1520-0493\(1997\)125<2821:DASOAM>2.0.CO;2](https://doi.org/10.1175/1520-0493(1997)125<2821:DASOAM>2.0.CO;2)
- Holt TR, Niyogi D, Chen F, Manning K, LeMone MA, Qureshi A (2006) Effect of land–atmosphere interactions on the IHOP 24–25 May 2002 convection case. *Mon Weather Rev* 134(1):113–133. <https://doi.org/10.1175/MWR3057.1>
- Hopsch SB, Thorncroft CD, Tyle KR (2010) Analysis of African easterly wave structures and their role in influencing tropical cyclogenesis. *Mon Weather Rev* 138(4):1399–1419. <https://doi.org/10.1175/2009MWR2760.1>
- Houze RA Jr (1993) *Cloud dynamics*. Academic, San Diego, p 573
- Hsieh J-S, Cook KH (2005) Generation of African easterly wave disturbances: relationship to the African easterly jet. *Mon Weather Rev* 133:1311–1327. <https://doi.org/10.1175/MWR2916.1>
- Hsieh J-S, Cook KH (2007) A study of the energetics of African easterly waves using a regional climate model. *J Atmos Sci* 64:421–440. <https://doi.org/10.1175/JAS3851.1>
- Hsieh J-S, Cook KH (2008) On the instability of the African easterly jet and the generation of African waves: reversals of the potential vorticity gradient. *J Atmos Sci* 65:2130–2151. <https://doi.org/10.1175/JAS2552.1>
- Huffman GJ, Adler RF, Bolvin DT, Gu G, Nelkin EJ, Bowman KP, Hong Y, Stocker EF, Wolff DB (2007) The TRMM multisatellite precipitation analysis (TMPA): quasi-global, multiyear, combined-sensor precipitation estimates at fine scales. *J Hydrometeorol* 8:38–55. <https://doi.org/10.1175/JHM560.1>
- Issa Lélé M, Lamb PJ (2010) Variability of the intertropical front (ITF) and rainfall over the West African Sudan–Sahel zone. *J Clim* 23(14):3984–4004. <https://doi.org/10.1175/2010JCLI3277.1>
- Jackson B, Nicholson SE, Klotter D (2009) Mesoscale convective systems over western equatorial Africa and their relationship to large-scale circulation. *Mon Weather Rev* 137(4):1272–1294. <https://doi.org/10.1175/2008MWR2525.1>
- Janiga MA, Thorncroft CD (2014) Convection over tropical Africa and the east Atlantic during the West African monsoon: regional and diurnal variability. *J Clim* 27(11):4159–4188. <https://doi.org/10.1175/JCLI-D-13-00449.1>
- Jiang H, Zipser EJ (2010) Contribution of tropical cyclones to the global precipitation from eight seasons of TRMM data: regional, seasonal, and interannual variations. *J Clim* 23(6):1526–1543. <https://doi.org/10.1175/2009JCLI3303.1>
- Jiang H, Liu C, Zipser EJ (2011) A TRMM-based tropical cyclone cloud and precipitation feature database. *J Appl Meteor Climatol* 50(6):1255–1274. <https://doi.org/10.1175/2011JAMC2662.1>
- Jirak IL, Cotton WR, McAnelly RL (2003) Satellite and radar survey of mesoscale convective system development. *Mon Weather Rev* 131(10):2428–2449. [https://doi.org/10.1175/1520-0493\(2003\)131<2428:SARSOM>2.0.CO;2](https://doi.org/10.1175/1520-0493(2003)131<2428:SARSOM>2.0.CO;2)
- Knippertz P, Fink AH (2008) Dry-season precipitation in tropical West Africa and its relation to forcing from the extratropics. *Mon Weather Rev* 136(9):3579–3596. <https://doi.org/10.1175/2008MWR2295.1>
- Knippertz P, Fink AH (2009) Prediction of dry-season precipitation in tropical West Africa and its relation to forcing from the extratropics. *Weather Forecasting* 24(4):1064–1084. <https://doi.org/10.1175/2009WAF2222221.1>
- Laing AG, Fritsch JM (1993) Mesoscale convective complexes in Africa. *Mon Weather Rev* 121: 2254–2263. [https://doi.org/10.1175/1520-0493\(1993\)121<2254:MCCIA>2.0.CO;2](https://doi.org/10.1175/1520-0493(1993)121<2254:MCCIA>2.0.CO;2)
- Laing AG, Fritsch JM, Negri AJ (1999) Contribution of mesoscale convective complexes to rainfall in Sahelian Africa: estimates from geostationary infrared and passive microwave data. *J Appl Meteorol* 38:957–964. [https://doi.org/10.1175/1520-0450\(1999\)038<0957:COMCCT>2.0.CO;2](https://doi.org/10.1175/1520-0450(1999)038<0957:COMCCT>2.0.CO;2)
- Laing AG, Carbone R, Levizzani V, Tuttle J (2008) The propagation and diurnal cycles of deep convection in northern tropical Africa. *Q J Roy Meteorol Soc* 134:93–109. <https://doi.org/10.1002/qj.194>
- Laing AG, Carbone RE, Levizzani V (2011) Cycles and propagation of deep convection over equatorial Africa. *Mon Weather Rev* 139(9):2832–2853. <https://doi.org/10.1175/2011MWR3500.1>
- Landsea CW, Gray WM (1992) The strong association between western Sahelian monsoon rainfall and intense Atlantic hurricanes. *J Clim* 5(5):435–453. [https://doi.org/10.1175/1520-0442\(1992\)005<0435:TSABWS>2.0.CO;2](https://doi.org/10.1175/1520-0442(1992)005<0435:TSABWS>2.0.CO;2)
- Laurent H, D’Amato N, Lebel T (1998) How important is the contribution of the mesoscale convective complexes to the Sahelian rainfall? *Phys Chem Earth* 23:629–633. [https://doi.org/10.1016/S0079-1946\(98\)00099-8](https://doi.org/10.1016/S0079-1946(98)00099-8)
- Liu C, Zipser EJ (2009) “Warm rain” in the tropics: seasonal and regional distributions based on 9 year of TRMM data. *J Clim* 22(3):767–779. <https://doi.org/10.1175/2008JCLI2641.1>
- Liu C, Zipser EJ, Cecil DJ, Nesbitt SW, Sherwood S (2008) A cloud and precipitation feature database from 9 years of TRMM observations. *J Appl Meteor Climatol* 47(10):2712–2728. <https://doi.org/10.1175/2008JAMC1890.1>
- Machado LAT, Duvel JP, Desbois M (1993) Diurnal variations and modulation by easterly waves of the size distribution of convective cloud clusters over West Africa and the Atlantic Ocean. *Mon Weather Rev* 121(1):37–49. [https://doi.org/10.1175/1520-0493\(1993\)121<0037:DVAMBE>2.0.CO;2](https://doi.org/10.1175/1520-0493(1993)121<0037:DVAMBE>2.0.CO;2)
- Maddox RA (1980) Mesoscale convective complexes. *Bull Am Meteorol Soc* 61:1374–1387. [https://doi.org/10.1175/1520-0477\(1980\)061<1374:MCC>2.0.CO;2](https://doi.org/10.1175/1520-0477(1980)061<1374:MCC>2.0.CO;2)
- Marshall JH, Dixon NS, Garcia-Carreras L, Lister G, Parker DJ, Knippertz P, Birch CE (2013) The role of moist convection in the West African monsoon system: insights from continental-scale convection-permitting simulations. *Geophys Res Lett* 40(9):1843–1849. <https://doi.org/10.1002/grl.50347>
- Mathon V, Laurent H, Lebel T (2002) Mesoscale convective system rainfall in the Sahel. *J Appl Meteorol* 41:1081–1092. [https://doi.org/10.1175/1520-0450\(2002\)041<1081:MCSRIT>2.0.CO;2](https://doi.org/10.1175/1520-0450(2002)041<1081:MCSRIT>2.0.CO;2)
- Maurer V, Bischoff-Gauß I, Kalthoff N, Gantner L, Roca R, Panitz HJ (2016) Initiation of deep convection in the Sahel in a convection-permitting climate simulation for northern Africa. *Q J R Meteorol Soc* 143(703):806–816. <https://doi.org/10.1002/qj.2966>
- Mbourou GNT, Bertrand JJ, Nicholson SE (1997) The diurnal and seasonal cycles of wind-borne dust over Africa north of the equator. *J Appl Meteorol* 36(7):868–882. [https://doi.org/10.1175/1520-0450\(1997\)036<0868:TDASCO>2.0.CO;2](https://doi.org/10.1175/1520-0450(1997)036<0868:TDASCO>2.0.CO;2)
- Miyakawa T, Satomura T (2006) Seasonal variation and environmental properties of southward propagating mesoscale convective systems over the Bay of Bengal. *SOLA* 2:88–91. <https://doi.org/10.2151/sola.2006-023>
- Mohr KI (2004) Interannual, monthly, and regional variability in the wet season diurnal cycle of precipitation in sub-Saharan Africa. *J Clim* 17:2441–2453. [https://doi.org/10.1175/1520-0442\(2004\)017<2441:IMARVI>2.0.CO;2](https://doi.org/10.1175/1520-0442(2004)017<2441:IMARVI>2.0.CO;2)
- Mohr KI, Thorncroft CD (2006) Intense convective systems in West Africa and their relationship to the African easterly jet. *Q J Roy Meteorol Soc* 132:163–176. <https://doi.org/10.1256/qj.05.55>
- Mohr KI, Zipser EJ (1996) Mesoscale convective systems defined by their 85-GHz ice scattering signature: size and intensity comparison over tropical oceans and continents. *Mon Weather Rev* 124:2417–2437. [https://doi.org/10.1175/1520-0493\(1996\)124<2417:MCSDBT>2.0.CO;2](https://doi.org/10.1175/1520-0493(1996)124<2417:MCSDBT>2.0.CO;2)

- Mohr KI, Famiglietti JS, Zipser EJ (1999) The contribution to tropical rainfall with respect to convective system type, size, and intensity estimated from the 85-GHz ice-scattering signature. *J Appl Meteorol* 38:596–606. [https://doi.org/10.1175/1520-0450\(1999\)038<0596:TCTTRW>2.0.CO;2](https://doi.org/10.1175/1520-0450(1999)038<0596:TCTTRW>2.0.CO;2)
- Nesbitt SW, Zipser EJ (2003) The diurnal cycle of rainfall and convective intensity according to 3 years of TRMM measurements. *J Clim* 16:1456–1475. <https://doi.org/10.1175/1520-0442&a>2.0.CO;2>
- Nesbitt SW, Zipser EJ, Cecil DJ (2000) A census of precipitation features in the tropics using TRMM: radar, ice scattering, and lightning observations. *J Clim* 13(23):4087–4106. [https://doi.org/10.1175/1520-0442\(2000\)013<4087:ACOPFI>2.0.CO;2](https://doi.org/10.1175/1520-0442(2000)013<4087:ACOPFI>2.0.CO;2)
- Nesbitt SW, Cifelli R, Rutledge SA (2006) Storm morphology and rainfall characteristics of TRMM precipitation features. *Mon Weather Rev* 134(10):2702–2721. <https://doi.org/10.1175/MWR3200.1>
- Nicholls SD, Mohr KI (2010) An analysis of the environments of intense convective systems in West Africa in 2003. *Mon Weather Rev* 138(10):3721–3739. <https://doi.org/10.1175/2010MWR332.1.1>
- Payne SW, McGarry MM (1977) The relationship of satellite inferred convective activity to easterly waves over West Africa and the adjacent ocean during phase III of GATE. *Mon Weather Rev* 105(4):413–420. [https://doi.org/10.1175/1520-0493\(1977\)105<0413:TROSIC>2.0.CO;2](https://doi.org/10.1175/1520-0493(1977)105<0413:TROSIC>2.0.CO;2)
- Pielke RA (2001) Influence of the spatial distribution of vegetation and soils on the prediction of cumulus convective rainfall. *Rev Geophys* 39(2):151–177. <https://doi.org/10.1029/1999RG000072>
- Provod M, Marsham JH, Parker DJ, Birch CE (2016) A characterization of cold pools in the West African Sahel. *Mon Weather Rev* 144(5):1923–1934. <https://doi.org/10.1175/MWR-D-15-0023.1>
- Pu B, Cook KH (2010) Dynamics of the West African westerly jet. *J Clim* 23:6263–6276. <https://doi.org/10.1175/2010JCLI3648.1>
- Pu B, Cook KH (2012) Role of the West African westerly jet in Sahel rainfall variations. *J Clim* 25:2880–2896. <https://doi.org/10.1175/JCLI-D-11-00394.1>
- Reed RJ, Norquist DC, Recker EE (1977) The structure and properties of African wave disturbances as observed during Phase III of GATE. *Mon Weather Rev* 105:317–333. [https://doi.org/10.1175/1520-0493\(1977\)105<0317:TSAPOA>2.0.CO;2](https://doi.org/10.1175/1520-0493(1977)105<0317:TSAPOA>2.0.CO;2)
- Schwanghart W, Schütt B (2008) Meteorological causes of Harmattan dust in West Africa. *Geomorphology* 95(3):412–428. <https://doi.org/10.1016/j.geomorph.2007.07.002>
- Shinoda M, Okatani T, Saloum M (1999) Diurnal variations of rainfall over Niger in the West African Sahel: a comparison between wet and drought years. *Int J Climatol* 19(1):81–94. [https://doi.org/10.1002/\(SICI\)1097-0088\(199901\)19:1,81:AID-JOC350.3.0.CO;2-F](https://doi.org/10.1002/(SICI)1097-0088(199901)19:1,81:AID-JOC350.3.0.CO;2-F)
- Sultan B, Janicot S (2003) The West African monsoon dynamics. Part II: The “preonset” and “onset” of the summer monsoon. *J Clim* 16(21):3407–3427. [https://doi.org/10.1175/1520-0442\(2003\)016<3407:TWAMDP>2.0.CO;2](https://doi.org/10.1175/1520-0442(2003)016<3407:TWAMDP>2.0.CO;2)
- Taylor CM, Birch CE, Parker DJ, Dixon N, Guichard F, Nikulin G, Lister GMS (2013) Modeling soil moisture-precipitation feedback in the Sahel: Importance of spatial scale versus convective parameterization. *Geophys Res Lett* 40:6213–6218. <https://doi.org/10.1002/2013GL058511>
- Tuttle JD, Carbone RE (2004) Coherent regeneration and the role of water vapor and shear in a long-lived convective episode. *Mon Weather Rev* 132(1):192–208. [https://doi.org/10.1175/1520-0493\(2004\)132<0192:CRATRO>2.0.CO;2](https://doi.org/10.1175/1520-0493(2004)132<0192:CRATRO>2.0.CO;2)
- Vizy EK, Cook KH (2017) Mesoscale convective systems and nocturnal rainfall over the West African Sahel: role of the Inter-tropical front. *Clim Dyn*. <https://doi.org/10.1007/s00382-017-3628-7>
- Yang GY, Slingo J (2001) The diurnal cycle in the tropics. *Mon Weather Rev* 129(4):784–801. [https://doi.org/10.1175/1520-0493\(2001\)129<0784:TDCITT>2.0.CO;2](https://doi.org/10.1175/1520-0493(2001)129<0784:TDCITT>2.0.CO;2)
- Zhang G, Cook KH, Vizy EK (2016a) The diurnal cycle of warm season rainfall over West Africa. Part I: observational analysis. *J Clim* 29(23):8423–8437. <https://doi.org/10.1175/JCLI-d-15-0874.1>
- Zhang G, Cook KH, Vizy EK (2016b) The diurnal cycle of warm season rainfall over West Africa. Part II: convection-permitting simulations. *J Clim* 29(23):8439–8454. <https://doi.org/10.1175/JCLI-d-15-0875.1>